INT. J. CONTROL, 2000, VOL. 73, NO. 3, 225–241

Compliant motion control for non-redundant rigid robotic manipulators

A. LANZON†* and R. J. RICHARDS†

A novel robust trajectory/force controller is developed on the basis of a combination of sliding-mode and adaptive control techniques. Exact knowledge of robot dynamics and environment stiffness is not required. The controller is constructed so as to track reference trajectories in the unconstrained directions and to regulate force at a desired value in the constrained directions. Changes in constraints are also taken into account in the design of the control law. The synthesis presented assumes a non-redundant rigid manipulator and known location/geometry of the environment. Simulation and experimental results are also presented.

1. Introduction

Many applications of robot manipulators to date have been based on position control. Hereafter, *position* is used to mean position and/or orientation, and *force* to mean force and/or torque. However, when a robot manipulator makes contact with an external surface (from now on referred to as the environment), control of both force and position is required. Position control strategies are adequate for tasks such as material transfer and spot welding where the manipulator is not interacting significantly with the environment. However, tasks such as assembly, fine polishing, grasping, grinding and deburring, which involve extensive contact with the environment, are better handled by directly controlling the forces of interaction between the manipulator and the environment. The task then is to exert a desired profile of force in the constrained degrees of freedom while following the reference trajectory in the unconstrained degrees of freedom (Whitney 1987). This problem is generally referred to as the *compliant motion control* problem.

The problem is non-trivial because the location and geometry of the environment are usually not well known; the environment stiffness is also usually unknown; force control on very stiff environments may lead to instability known as hard contact instability; trajectory tracking and force regulation must occur in the presence of model uncertainty and disturbances, the controller must be capable of handling changes in constraints (i.e. collision phenomena must be taken into account); the force measurement is usually very noisy, thus prohibiting force derivatives to be computed; and ways must be found of combining force control commands and position control commands when regulating force in a direction normal to the environment and following a trajectory along the environment.

Received 30 July 1998.

* Author for correspondence. e-mail: AL225@eng.cam.ac.uk

† Department of Engineering, University of Cambridge, Cambridge CB2 1PZ, UK.

The compliant motion control problem has attracted considerable attention over the past two decades. Currently available compliant motion control techniques may be categorized into two basic types. One is passive compliance, where some 'soft' device is inserted near the end-effector. This can be the force sensor itself. Whitney (1987) showed that a soft force sensor can lead to stable behaviour with stiff environments. However, drawbacks of soft sensors include the reduction in dynamic range of the force response and positional accuracy. The most well known passive compliance device is the remote center of compliance (RCC) (Whitney and Rourke 1986). The other compliant motion control category is active compliance where compliance is achieved through joint-torques, either by setting a linear relation between the force and displacement (or force and velocity) such as impedance control (Hogan 1984), damping control (Whitney 1977), stiffness control (Salisbury 1980) and resolved acceleration control (Luh *et al.* 1980); or by controlling force in certain directions while controlling position in the remaining directions, such as hybrid control (Raibert and Craig 1981), compliance and force control (Mason 1981) and compliance control (Paul and Shimano 1982).

Most of the force control schemes mentioned in the above references have been devised on cartesian coordinates at the end-effector or at an external compliance frame. The rationale for cartesian position/force control is that the geometry of the external world defines a set of natural coordinates that can be partitioned into position-controlled variables and force-controlled variables (Mason 1981, Lipkin and Duffy 1986). Control, therefore, is cast in terms of these variables, necessitating a kinematic transformation to joint variables. Care must be taken to ensure that the kinematic instabilities recently explained by Fisher and Mujtaba (1992) and previously seen by An and Hollerbach (1987) and Zhang (1989) are well avoided.

In this paper, the problem is addressed through a combination of adaptive and sliding-mode control techniques. Sliding-mode control is a natural candidate for

this problem because it is a robust technique which explicitly takes care of the non-linear plant dynamics. It gives robustness against parametric uncertainty and unmodelled dynamics in the sense that it ensures bounded trajectory tracking errors and force regulation errors in the presence of bounded uncertainty. Adaptation is used only to estimate the unknown environment stiffness. This is estimated through an adaptive algorithm, rather than by designing a controller which is robust to its variations, because it varies considerably (typically, from 10^4 to $10^8\,\mathrm{N\,m^{-1}}$) depending on the material from which the environment is made. Hereafter, *trajectory tracking* is used to mean the position and velocity tracking of a reference trajectory given in task space. Other authors have also considered a similar problem. Probably, the most significant papers are by Chiaverini and Sciavicco (1993), Lu and Goldenberg (1995), Colbaugh *et al.* (1995), Seraji and Colbaugh (1997), Chiaverini *et al.* (1998) and Seraji (1998).

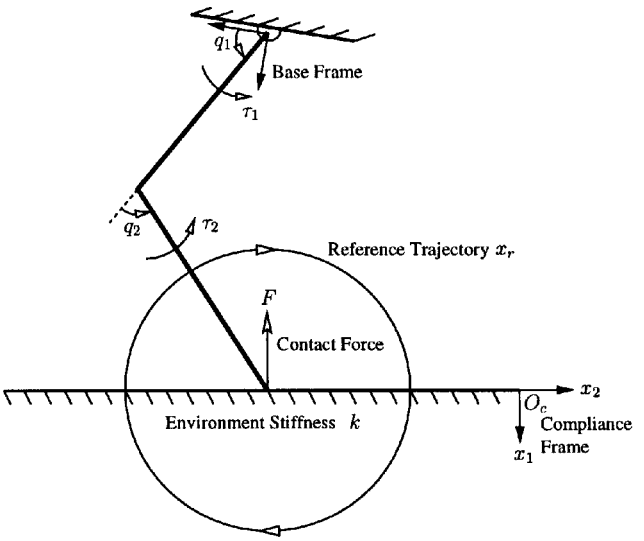

Figure 1. 2-D planar manipulator arm.

2. Problem formulation

The problem considered here is that of controlling a general n-degree of freedom non-redundant rigid manipulator to track reference trajectories in the unconstrained directions, and to regulate force at a desired value in the constrained directions—in the presence of model uncertainty and unknown environment stiffness. If there are no constrained directions, then pure trajectory tracking should be achieved; whereas if there are no unconstrained directions, then pure force control should be achieved. A further issue which is addressed is that of ensuring stability whenever one or more constraints change.

Consider the 2-D planar manipulator arm illustrated in figure 1, which is useful for depicting notation. All subsequent theory is valid for any non-redundant manipulator with n-degrees of freedom. Non-redundancy is required so that the manipulator Jacobian is square. Here, let q be the vector of joint displacements, τ be the vector of joint torques, $H(q)$ be the manipulator inertia matrix, and the non-linear term $h(q,\dot{q})$ contain centrifugal, coriolis and gravitational forces. Furthermore, let $J_o(q)$ denote the manipulator Jacobian and F_o (a three-component vector) be the environment reaction force read with respect to the base coordinate system. Also, let ${}^oR_c$ denote the rotation matrix which transforms vectors read with respect to the compliance frame to vectors read with respect to the base coordinate system. Then, the manipulator dynamics in joint space are given by (Murray *et al.* 1994)

$$H(q)\ddot{q} + h(q,\dot{q}) = \tau + J_o^{\mathrm{T}}(q)F_o \tag{1}$$

$$\Rightarrow\quad H(q)\ddot{q} + h(q,\dot{q}) = \tau + J_o^{\mathrm{T}}(q)({}^oR_cF) \tag{2}$$

where F is measured in the compliance frame. Now let $\mathrm{d}q$ be a differential change in the joint displacements, $\mathrm{d}x_o$ be the corresponding differential change in end-effector position read with respect to the base coordinate system and $\mathrm{d}x$ be the same differential change in end-effector position but read in the compliance coordinate system. Then $\mathrm{d}x_o = J_o\,\mathrm{d}q$ and $\mathrm{d}x = {}^cR_o\,\mathrm{d}x_o$, implying $\mathrm{d}x = ({}^cR_oJ_o)\,\mathrm{d}q$. Hence $({}^cR_oJ_o)$ is the Jacobian of the transformation mapping *joint space* to *task space*. Denote this transformation Jacobian by $J(q)$. Then we have $J^{\mathrm{T}}(q) = J_o^{\mathrm{T}}(q)\,{}^cR_o^{\mathrm{T}} = J_o^{\mathrm{T}}(q)\,{}^oR_c$ and so equation (2) gives

$$H(q)\ddot{q} + h(q,\dot{q}) = \tau + J^{\mathrm{T}}(q)F \tag{3}$$

Now let x be the position vector of the end-effector measured from the compliance frame and $\Upsilon(\cdot)$ be the kinematic transformation mapping joint space to task space ($\Upsilon : \mathbb{R}^n \to \mathbb{R}^n$ is a non-linear function). Then

$$\left.\begin{aligned} x &= \Upsilon(q) && \Rightarrow\ q = \Upsilon^{-1}(x)\\ \dot{x} &= J(q)\dot{q} && \Rightarrow\ \dot{q} = J(q)^{-1}\dot{x}\\ \ddot{x} &= J(q)\ddot{q} + \dot{J}(q)\dot{q} && \Rightarrow\ \ddot{q} = J(q)^{-1}(\ddot{x} - \dot{J}(q)\dot{q}) \end{aligned}\right\} \tag{4}$$

Here it is assumed that the manipulator arm does not pass through a manipulator singularity. This is necessary so that inverse transformations are possible and can be ensured by monitoring the magnitude of the joint torques/velocities. Note that non-redundancy means that $\dim q = \dim x = n$. The transformation $\Upsilon(\cdot)$ is composed of the forward kinematics, describing the end-effector position with respect to the base coordinate system in terms of the joint angles, and a homogeneous transformation, mapping this position read with respect to the base coordinates to the compliance frame. As shown above, the Jacobian $J(q)$ is the Jacobian of the transformation $\Upsilon(\cdot)$. It is not the same as the manipu-

lator Jacobian $J_o(q)$. In fact, from above, $J(q) = {}^{c}R_o J_o(q)$. Dropping the operands for clarity (they are all in joint space) results in

$$H\ddot{q} + h = \tau + J^{\mathrm{T}}F$$

$$(4) \Rightarrow HJ^{-1}(\ddot{x} - \dot{J}\dot{q}) + h = \tau + J^{\mathrm{T}}F$$

Applying the partial feedback linearization control law

$$\tau = \hat{H}\hat{J}^{-1}(u - \hat{\dot{J}}\dot{q}) + \hat{h} - \hat{J}^{\mathrm{T}}F \qquad (5)$$

where $\hat{H}$, $\hat{h}$ and $\hat{J}$ are estimates of H, h and J respectively and u represents a new input to the system which is yet to be chosen, in turn gives

$$HJ^{-1}(\ddot{x} - \dot{J}\dot{q}) + h - J^{\mathrm{T}}F = \hat{H}\hat{J}^{-1}(u - \hat{\dot{J}}\dot{q}) + \hat{h} - \hat{J}^{\mathrm{T}}F$$

which on rearrangement [H is always positive definite (Kwan 1995) and hence invertible] gives

$$\ddot{x} = JH^{-1}\hat{H}\hat{J}^{-1}u + JH^{-1}[(HJ^{-1}\dot{J} - \hat{H}\hat{J}^{-1}\hat{\dot{J}})\dot{q} + (\hat{h} - h)] + JH^{-1}(J^{\mathrm{T}} - \hat{J}^{\mathrm{T}})F \qquad (6)$$

Note that the terms in the above equation are matrix/vector functions of q and $\dot{q}$. Now, equations (4) give $q = \Upsilon^{-1}(x)$ and $\dot{q} = J(q)^{-1}\dot{x}$, and so by letting $X = (x^{\mathrm{T}}, \dot{x}^{\mathrm{T}})^{\mathrm{T}}$ and defining

$$\left.\begin{aligned} G(X) &= JH^{-1}\hat{H}\hat{J}^{-1} \\ f(X) &= JH^{-1}[HJ^{-1}\dot{J} - \hat{H}\hat{J}^{-1}\hat{\dot{J}})\dot{q} + (\hat{h} - h)] \\ M(X) &= JH^{-1}(J^{\mathrm{T}} - \hat{J}^{\mathrm{T}}) \end{aligned}\right\} \qquad (7)$$

equation (6) becomes

$$\ddot{x} = G(X)u + f(X) + M(X)F \qquad (8)$$

Here $x, u, F \in \mathbb{R}^n$, $X = (x^{\mathrm{T}}, \dot{x}^{\mathrm{T}})^{\mathrm{T}} \in \mathbb{R}^{2n}$, $f : \mathbb{R}^{2n} \to \mathbb{R}^n$ and $G, M : \mathbb{R}^{2n} \to \mathbb{R}^{n \times n}$. Equation (8) is now suitable for sliding-mode controller synthesis (Slotine and Li 1991). Designing a controller for this equation immediately yields a controller for the robot arm $H(q)\ddot{q} + h(q, \dot{q}) = \tau + J_o^{\mathrm{T}}(q)F_o$, since equation (5) provides a mapping from the control input u to the torque input τ.

3. Controller structure

As seen in § 2, substituting equation (5) into the manipulator dynamical equation (1) gives the new system described by equation (8). This is illustrated in figure 2. Thus, the problem of designing a controller for the robot dynamics of (1) reduces to the problem of designing a controller for this 'new plant' described by equation (8). Note that if the robot dynamics were known perfectly, then $G(X) = I$, $f(X) = 0$ and $M(X) = 0$, yielding the simple uncoupled dynamical equation $\ddot{x} = u$. In this case, the controller synthesis is trivial and can be adequately handled by standard linear

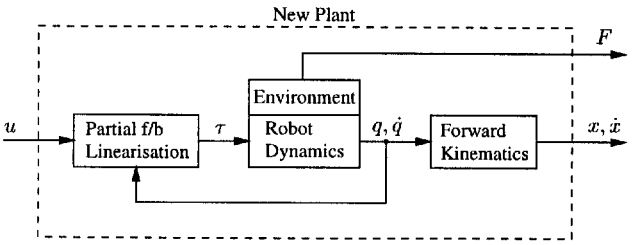

Figure 2. New plant given by equation (8).

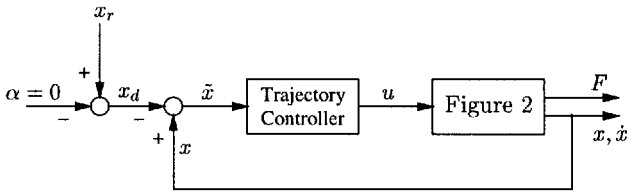

Figure 3. Trajectory-tracking controller.

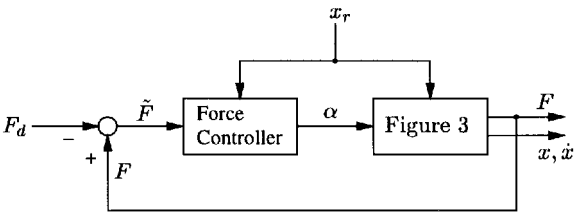

Figure 4. Trajectory-tracking and force-regulating controller.

control theory. However, in general, this is not the case and a more sophisticated (possibly non-linear) control law which explicitly takes into account the above dynamics must be sought. The control challenge then is to: (a) design a control law u to effectively account for parameter uncertainty and the presence of high-frequency unmodelled dynamics, and (b) explicitly quantify the resulting modelling/performance trade-offs. These issues are addressed here by using the concepts and notations of sliding-mode control theory.

To solve the compliant motion control problem, the two main objectives are to track the reference trajectory in the unconstrained directions, and to regulate the force in the constrained directions. The problem of trajectory tracking can be solved by designing a sliding-mode controller of the form illustrated in figure 3. Here $\alpha = 0$, so that $x_{\mathrm{d}}(t) = x_{\mathrm{r}}(t)$ (i.e. the desired trajectory is equal to the reference trajectory). $\alpha(t)$ is an internal control signal which will be non-zero when the system is in force control. Treating the whole closed-loop system in figure 3 as a new plant, a sliding-mode force-regulating controller can be designed around it to achieve the second objective. In this case, $\alpha(t)$ will in general be non-zero. This structure is shown in figure 4. In this figure, F_{d} denotes the desired contact force. It is important to note that force control is not simply achieved by the force-regulating controller giving positional com-

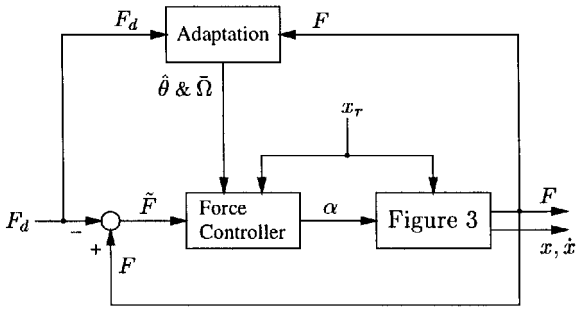

Figure 5. Simplified overall structure.

mands to the trajectory-tracking controller and the latter controlling the plant since both the force controller and the trajectory-tracking controller share some common terms which are not easy to show diagrammatically. Hence both controllers interact and are not completely separate entities. Finally, since the environment stiffness is unknown in practice, an adaptive algorithm is designed to estimate this. The overall simplified structure is shown in figure 5. In this figure, $\hat{\theta}$ and $\bar{\Omega}$ are adaptation parameters which will be defined later.

4. Controller design

The controller is derived in two steps. In the first step the environment stiffness is assumed to be completely known, and in the second step an adaptive algorithm is derived to relax this assumption. The reader is referred to Lanzon (1997) for a more detailed derivation.

4.1. *Known environment stiffness*

Consider the multiple-input multiple-output system of equation (8). Let the components of $f(X)$ be denoted by $f(X)_i$ and the elements of $G(X)$ and $M(X)$ be $g(X)_{ij}$ and $m(X)_{ij}$ respectively. Here u is the control input, $X = (x^{\mathrm{T}}, \dot{x}^{\mathrm{T}})^{\mathrm{T}}$ is the state-vector—wherein x is the output position and F is the reaction force exerted by an environment placed at $x = 0$ and having environment stiffness k. There is no loss of generality in assuming that the environment is located at $x = 0$. For small deformations, the contact force can be modelled as an elastic force as follows

$$F_i = \begin{cases} -kx_i & \text{if } x_i \geq 0 \\ 0 & \text{otherwise} \end{cases}$$

Expressing equation (8) in component form yields

$$\ddot{x}_i = g(X)_{ii}u_i + [f(X)_i + c_i(X, u, F)] + m(X)_{ii}F_i \quad (9)$$

where $c_i(X, u, F) = \sum_{j \neq i}[g(X)_{ij}u_j + m(X)_{ij}F_j]$.

$G(X)$, $f(X)$ and $M(X)$ are, in general, non-linear matrix functions of the state. They are not exactly known but the extent of imprecision from their nominal functions $\hat{G}(X)$, $\hat{f}(X)$ and $\hat{M}(X)$ is bounded by some specified functions. As seen from equations (7), the estimates $\hat{G}(X)$, $\hat{f}(X)$ and $\hat{M}(X)$ to the uncertain matrix functions $G(X)$, $f(X)$ and $M(X)$ are I, 0 and 0 respectively. So the nominal functions are given by

$$\begin{aligned} \hat{G}(X) = I \quad &\Rightarrow \quad \hat{g}(X)_{ii} = 1, \hat{g}(X)_{ij}|_{j \neq i} = 0 \\ \hat{f}(X) = 0 \quad &\Rightarrow \quad \hat{f}(X)_i = 0 \\ \hat{M}(X) = 0 \quad &\Rightarrow \quad \hat{m}(X)_{ij} = 0 \end{aligned}$$

Also, the uncertain matrix functions $f(X)$, $M(X)$ and $G(X)$ are bounded *component-wise* by the matrix functions $U : \mathbb{R}^{2n} \to \mathbb{R}^n$, $W : \mathbb{R}^{2n} \to \mathbb{R}^{n \times n}$ and $V : \mathbb{R}^{2n} \to \mathbb{R}^{n \times n}$ respectively as follows

$$\begin{aligned} V(X)_{ii}^{-1} \leq \frac{g(X)_{ii}}{\hat{g}(X)_{ii}} \leq V(X)_{ii} \\ [j \neq i] \quad |g(X)_{ij} - \hat{g}(X)_{ij}| \leq V(X)_{ij} \\ |f(X)_i - \hat{f}(X)_i| \leq U(X)_i \\ |m(X)_{ij} - \hat{m}(X)_{ij}| \leq W(X)_{ij} \end{aligned}$$

where $U(X)_i$ are the components of $U(X)$ and $W(X)_{ij}$ and $V(X)_{ij}$ are the elements of $W(X)$ and $V(X)$ respectively. Here it is assumed that $g(X)_{ii} > 0$.† Note that $V(X)_{ii} \geq 1$, for if it were < 1, then $V(X)_{ii}^{-1} > V(X)_{ii}$ which, according to the above, is not sensible. $g(X)_{ii}$ is bounded differently from $g(X)_{ij}$ [when $j \neq i$] because $g(X)_{ij}$ is a coupling term, as seen from equation (9).

Let λ be a scalar design parameter which can be interpreted as the desired control bandwidth (Asada and Slotine 1986, p.141). Define $\tilde{x} = x - x_{\mathrm{d}}$ as the error between the actual position and the desired position, and let the desired position x_{d} be obtained by subtracting some internal control signal $\alpha(t)$ from the reference signal x_{r} (i.e. $x_{\mathrm{d}} = x_{\mathrm{r}} - \alpha$). Thus $x_{\mathrm{d}}, x_{\mathrm{r}}, \alpha \in \mathbb{R}^n$. It will be seen that $\alpha(t)$ plays an important role in force control. $\alpha(t) = 0$ during trajectory tracking, hence giving $x_{\mathrm{d}}(t) = x_{\mathrm{r}}(t)$, and varies so that force regulation is achieved when the system is in contact with the environment. Furthermore, define $\tilde{X} = (\tilde{x}^{\mathrm{T}}, \dot{\tilde{x}}^{\mathrm{T}})^{\mathrm{T}}$ as the state-vector for the error dynamics. Formally let the variables of interest be $\int^t \tilde{x}_i \, \mathrm{d}T$ (where T is a dummy variable of integration) and define time-varying sliding surfaces $s_i(t)$ in state-spaces $\mathbb{R}^r$ by the scalar equations $s_i(X, t) = 0$, where

$$s_i = \left(\frac{\mathrm{d}}{\mathrm{d}t} + \lambda\right)^{r-1} \int^t \tilde{x}_i \, \mathrm{d}T \quad \text{with} \quad r = 3$$

The integral $\int^t \tilde{x}_i \, \mathrm{d}T$ is defined to within a constant as there is no lower limit of integration. The constant can

† This assumption is not restrictive as equations (5) and (8) can easily be rewritten so that $g(X)_{ii} > 0$. It only means that u_i contributes to $\ddot{x}_i$ with known sign.

be chosen such that $s_i(t=0) = 0$ *regardless of* $\tilde{X}(t=0)$. $\int^t \tilde{x}_i \, dT$ was chosen as the variable of interest rather than simply $\tilde{x}_i$ so as to augment the state-space by one dimension for each i and hence pass the sliding surface through the initial condition. In this case, the state is initially on the sliding surface and is not required to converge to the surface before sliding occurs. Here $r = 3$ as the system described by equation (9) is third-order with respect to the variable of interest $\int^t \tilde{x}_i \, dT$. Hence the surfaces $s_i(t) = 0$ are planes which lie in $\mathbb{R}^3$. An argument which shows that the choice of dynamics used to define the above sliding surface is the 'best-conditioned' among linear dynamics, in the sense that it guarantees the best tracking performance for a given desired control bandwidth and a given extent of parameter uncertainty, is given in Slotine and Li (1991). Thus

$$s_i = \dot{\tilde{x}}_i + 2\lambda\tilde{x}_i + \lambda^2 \int_o^t \tilde{x}_i \, dT \underbrace{- \dot{\tilde{x}}_i(0) - 2\lambda\tilde{x}_i(0)}_{\substack{\text{so that} \\ s_i = 0 \text{ at } t=0}} \tag{10}$$

giving

$$\begin{aligned} \dot{s}_i &= \ddot{\tilde{x}}_i + 2\lambda\dot{\tilde{x}}_i + \lambda^2\tilde{x}_i \\ &= \ddot{x}_i - \ddot{x}_{d_i} + 2\lambda\dot{\tilde{x}}_i + \lambda^2\tilde{x}_i \\ &= g(X)_{ii}u_i + [f(X)_i + c_i(X,u,F)] \\ &\quad + m(X)_{ii}F_i - \ddot{x}_{d_i} + 2\lambda\dot{\tilde{x}}_i + \lambda^2\tilde{x}_i \end{aligned}$$

Let 'sat' denote the saturation function, defined as $\operatorname{sat} y = y$ if $|y| \leq 1$ and $\operatorname{sat} y = y/|y|$ otherwise. Also, let Φ_i be the (non-constant) thickness of a boundary layer neighbouring the switching surface $s_i(t) = 0$. This boundary layer is required so that the switched control law, which causes control chattering, can be approximated by a continuous control law inside this boundary (Asada and Slotine 1986). By choosing

$$u_i = \ddot{x}_{d_i} - 2\lambda\dot{\tilde{x}}_i - \lambda^2\tilde{x}_i - \Psi_i \operatorname{sat}\frac{s_i}{\Phi_i} \tag{11}$$

where Ψ_i is the extent of non-linearity required to guarantee that state-trajectories outside the boundary layer converge to within the boundary layer, then

$$\begin{aligned} \dot{s}_i &= (g(X)_{ii} - 1)(\ddot{x}_{d_i} - 2\lambda\dot{\tilde{x}}_i - \lambda^2\tilde{x}_i) + f(X)_i \\ &\quad + c_i(X,u,F) + m(X)_{ii}F_i - g(X)_{ii}\Psi_i \operatorname{sat}\frac{s_i}{\Phi_i} \end{aligned} \tag{12}$$

When $|s_i| > \Phi_i$, all state-trajectories are required to converge to within the sliding region. This is ensured by satisfying the Lyapunov condition (Slotine and Li 1991, p. 293)

$$\tfrac{1}{2}\frac{d}{dt}s_i^2 = \dot{s}_i s_i \leq (\Phi_i - \eta)|s_i|$$

where η is a positive constant required to ensure that trajectories outside the boundary layer converge to within the sliding region in finite time. That is, it is required to satisfy

$$\begin{aligned} &(g(X)_{ii} - 1)(\ddot{x}_{d_i} - 2\lambda\dot{\tilde{x}}_i - \lambda^2\tilde{x}_i)s_i + f(X)_i s_i \\ &\quad + c_i(X,u,F)s_i + m(X)_{ii}F_i s_i - g(X)_{ii}\Psi_i|s_i| \\ &\qquad \leq (\Phi_i - \eta)|s_i| \end{aligned}$$

Thus, select Ψ_i such that

$$\begin{aligned} &(\Psi_i + g(X)_{ii}^{-1}\Phi_i - g(X)_{ii}^{-1}\eta)|s_i| \\ &\quad \geq |1 - g(X)_{ii}^{-1}||\ddot{x}_{d_i} - 2\lambda\dot{\tilde{x}}_i - \lambda^2\tilde{x}_i||s_i| \\ &\qquad + |g(X)_{ii}^{-1}|(|f(X)_i||s_i| + |m(X)_{ii}||F_i||s_i| \\ &\qquad + \sum_{j\neq i}(|g(X)_{ij}||u_j| + |m(X)_{ij}||F_j|)|s_i|) \end{aligned}$$

or, substituting uncertainty bounds with $\hat{g}(X)_{ii} = 1$, $\hat{g}(X)_{ij} = 0$, $\hat{f}(X)_i = 0$ and $\hat{m}(X)_{ij} = 0$,

$$\begin{aligned} \Psi_i \geq\ & (V(X)_{ii} - 1)\left|\ddot{x}_{d_i} - 2\lambda\dot{\tilde{x}}_i - \lambda^2\tilde{x}_i\right| \\ &+ V(X)_{ii}[\eta + U(X)_i + C_i(X,u,F) \\ &+ W(X)_{ii}|F_i|] - g(X)_{ii}^{-1}\Phi_i \end{aligned}$$

where $C_i(X,u,F) = \sum_{j\neq i}[V(X)_{ij}|u_j| + W(X)_{ij}|F_j|]$. The last term in the above inequality is not readily taken care of as Φ_i may be positive or negative. Consequently, by choosing

$$\begin{aligned} \Psi_i = &(V(X)_{ii} - 1)|\ddot{x}_{d_i} - 2\lambda\dot{\tilde{x}}_i - \lambda^2\tilde{x}_i| \\ &+ V(X)_{ii}[\eta + U(X)_i + C_i(X,u,F) \\ &+ W(X)_{ii}|F_i|] - V(X)_{ii}^{-\operatorname{sgn}\Phi_i}\Phi_i \end{aligned} \tag{13}$$

boundary layer attractiveness is ensured.

When $|s_i| \leq \Phi_i$, from equation (12)

$$\begin{aligned} &\dot{s}_i + \left(\frac{g(X)_{ii}\Psi_i}{\Phi_i}\right)s_i \\ &\quad = f(X)_i + c_i(X,u,F) + m(X)_{ii}F_i \\ &\qquad + (g(X)_{ii} - 1)(\ddot{x}_{d_i} - 2\lambda\dot{\tilde{x}}_i - \lambda^2\tilde{x}_i) \end{aligned} \tag{14}$$

Letting

$$\left(\frac{g(X)_{ii}\Psi_i}{\Phi_i}\right)_{\max} = \lambda$$

gives

$$[g(X)_{ii}]_{\max}\frac{\Psi_i}{\Phi_i} = \lambda \quad \Rightarrow \quad \Psi_i = V(X)_{ii}^{-1}\lambda\Phi_i \tag{15}$$

This condition is known as the balanced condition. It specifies the best tracking performance attainable, given the desired control bandwidth and the extent of parameter uncertainty (Slotine and Li 1991, p. 298). Using equation (15) in (13) results in

$$\Phi_i + V(X)_{ii}^{-1+\operatorname{sgn}\Phi_i}\lambda\Phi_i = V(X)_{ii}^{\operatorname{sgn}\Phi_i}(V(X)_{ii} - 1)\left|\ddot{x}_{d_i} - 2\lambda\dot{\tilde{x}}_i - \lambda^2\tilde{x}_i\right| + V(X)_{ii}^{1+\operatorname{sgn}\Phi_i}[\eta + U(X)_i + C_i(X,u,F) + W(X)_{ii}|F_i|] \quad (16)$$

Also, from equations (14), (15) and (16), note that s_i is a measure of the perturbation between the nominal model and the actual physical system whereas Φ_i is a measure of the uncertainty in the model.

From the above synthesis it can be seen that, when $\alpha_i = 0$, the control inputs make x_i follow x_{r_i}; hence *trajectory tracking* is achieved. Extending this argument, when $\alpha_i \neq 0$, the control inputs make x_i follow $x_{d_i}[= (x_{r_i} - \alpha_i)]$. Thus *force regulation* can be achieved if $\alpha_i(t)$ is varied such that F_i remains constant at F_d, when the system is in contact with the environment. One may attempt to find such an $\alpha_i(t)$ analytically as follows. Substituting the control input u_i from equation (11) into (9) gives

$$\ddot{x}_i = g(X)_{ii}(\ddot{x}_{d_i} - 2\lambda\dot{\tilde{x}}_i - \lambda^2\tilde{x}_i) + f(X)_i + c_i(X,u,F) + m(X)_{ii}F_i - g(X)_{ii}\Psi_i \operatorname{sat}\frac{s_i}{\Phi_i}$$

Putting $\ddot{x}_i = g(X)_{ii}\ddot{x}_i - (g(X)_{ii} - 1)\ddot{x}_i$ yields

$$g(X)_{ii}(\ddot{\tilde{x}}_i + 2\lambda\dot{\tilde{x}}_i + \lambda^2\tilde{x}_i) = (g(X)_{ii} - 1)\ddot{x}_i + f(X)_i + c_i(X,u,F) + m(X)_{ii}F_i - g(X)_{ii}\Psi_i \operatorname{sat}\frac{s_i}{\Phi_i}$$

which, on rearranging, gives

$$\ddot{\tilde{x}}_i + 2\lambda\dot{\tilde{x}}_i + \lambda^2\tilde{x}_i = (1 - g(X)_{ii}^{-1})\ddot{x}_i + g(X)_{ii}^{-1}[f(X)_i + c_i(X,u,F) + m(X)_{ii}F_i] - \Psi_i \operatorname{sat}\frac{s_i}{\Phi_i} \quad (17)$$

This equation represents the closed-loop dynamics of the system. Defining $\tilde{F}_i$ as the difference between the actual contact force and the desired contact force (i.e. $\tilde{F}_i = F_i - F_d$), then during contact (i.e. $x_i \geq 0$)

$$F_i = -kx_i, \qquad \tilde{F}_i = F_i - F_d$$
$$\dot{F}_i = -k\dot{x}_i, \qquad \dot{\tilde{F}}_i = \dot{F}_i = -k\dot{x}_i \quad [F_d = \text{const.}]$$
$$\ddot{F}_i = -k\ddot{x}_i, \qquad \ddot{\tilde{F}}_i = \ddot{F}_i = -k\ddot{x}_i$$

Since F is negative, the desired contact force F_d should also be defined negative. Note also that only one desired contact force is specified here. Substituting the above equations in (17) yields

$$\ddot{\tilde{F}}_i + 2\lambda\dot{\tilde{F}}_i + \lambda^2\tilde{F}_i = -\lambda^2 F_d - k\Big[(\ddot{x}_{r_i} + 2\lambda\dot{x}_{r_i} + \lambda^2 x_{r_i}) - (\ddot{\alpha}_i + 2\lambda\dot{\alpha}_i + \lambda^2\alpha_i) + (1 - g(X)_{ii}^{-1})\ddot{x}_i + g(X)_{ii}^{-1}[f(X)_i + c_i(X,u,F) + m(X)_{ii}F_i] - \Psi_i \operatorname{sat}\frac{s_i}{\Phi_i}\Big] \quad (18)$$

For asymptotic stability of $\tilde{F}_i$, it is sufficient to choose $\alpha_i(t)$ such that $\text{RHS} \equiv 0\ \forall t$ (during contact). However, practically this cannot be done since $g(X)_{ij}$, $f(X)_i$ and $m(X)_{ij}$ are uncertain and $\ddot{x}_i$ is difficult to measure. Again, taking a sliding-mode approach, formally let the variables of interest be $\int^t \tilde{F}_i/(-k)\,dT$ and define time-varying sliding surfaces $p_i(t)$ in state-spaces $\mathbb{R}^r$ by the scalar equations $p_i(X,t) = 0$, where

$$p_i = \left(\frac{d}{dt} + \lambda\right)^{r-1}\int^t \frac{\tilde{F}_i}{-k}\,dT \qquad \text{where } r = 3$$

Thus

$$(-kp_i) = \dot{\tilde{F}}_i + 2\lambda\tilde{F}_i + \lambda^2\int_o^t \tilde{F}_i\,dT \underbrace{-\dot{\tilde{F}}_i(0) - 2\lambda\tilde{F}_i(0)}_{\substack{\text{so that}\\ p_i=0 \text{ at } t=0}} \quad (19)$$

giving

$$\dot{p}_i = \frac{1}{-k}(\ddot{\tilde{F}}_i + 2\lambda\dot{\tilde{F}}_i + \lambda^2\tilde{F}_i)$$

Using equation (18), this becomes

$$\dot{p}_i = \frac{\lambda^2 F_d}{k} + (\ddot{x}_{r_i} + 2\lambda\dot{x}_{r_i} + \lambda^2 x_{r_i}) - (\ddot{\alpha}_i + 2\lambda\dot{\alpha}_i + \lambda^2\alpha_i) + (1 - g(X)_{ii}^{-1})\ddot{x}_i + g(X)_{ii}^{-1}[f(X)_i + c_i(X,u,F) + m(X)_{ii}F_i] - \Psi_i \operatorname{sat}\frac{s_i}{\Phi_i} \quad (20)$$

Similarly to above, let ϕ_i be the thickness of a boundary layer neighbouring the force control switching surface $p_i(t) = 0$ and let ψ_i be the extent of non-linearity required to ensure that state-trajectories outside this boundary layer converge to within it. Then, by choosing

$$\ddot{\alpha}_i + 2\lambda\dot{\alpha}_i + \lambda^2\alpha_i = \frac{\lambda^2 F_d}{k} + (\ddot{x}_{r_i} + 2\lambda\dot{x}_{r_i} + \lambda^2 x_{r_i}) - \Psi_i \operatorname{sat}\frac{s_i}{\Phi_i} + \psi_i \operatorname{sat}\frac{p_i}{\phi_i} \quad (21)$$

equation (20) becomes

$$\dot{p}_i = (1 - g(X)_{ii}^{-1})\ddot{x}_i + g(X)_{ii}^{-1}[f(X)_i + c_i(X,u,F) + m(X)_{ii}F_i] - \psi_i \operatorname{sat}\frac{p_i}{\phi_i}$$

Note that $\ddot{x}_i$ is difficult to measure. So substituting for $\ddot{x}_i$ from equation (9) gives

$$\dot{p}_i = (g(X)_{ii} - 1)u_i + f(X)_i + c_i(X,u,F) + m(X)_{ii}F_i - \psi_i \operatorname{sat}\frac{p_i}{\phi_i} \quad (22)$$

in which u_i is computable for all i.

By an analogous argument to above, when $|p_i| > \phi_i \Leftrightarrow |-kp_i| > (k\phi_i)$, state-trajectories are required to satisfy the Lyapunov condition

$$\tfrac{1}{2}\frac{d}{dt}p_i^2 = \dot{p}_i p_i = (g(X)_{ii} - 1)u_i p_i + f(X)_i p_i + c_i(X,u,F)p_i + m(X)_{ii}F_i p_i - \psi_i|p_i| \leq (\dot{\phi}_i - \eta)|p_i|$$

Thus ψ_i is selected such that

$$(\psi_i + \dot{\phi}_i - \eta)|p_i| \geq |g(X)_{ii} - 1||u_i||p_i| + \sum_{j\neq i}(|g(X)_{ij}||u_j| + |m(X)_{ij}||F_j|)|p_i| + |f(X)_i||p_i| + |m(X)_{ii}||F_i||p_i|$$

or, substituting the uncertainty bounds,

$$\psi_i \geq \eta + (V(X)_{ii} - 1)|u_i| + U(X)_i + C_i(X,u,F) + W(X)_{ii}|F_i| - \dot{\phi}_i$$

Hence, by choosing

$$\psi_i = \eta + (V(X)_{ii} - 1)|u_i| + U(X)_i + C_i(X,u,F) + W(X)_{ii}|F_i| - \dot{\phi}_i \quad (23)$$

boundary layer attractiveness is ensured as before.

When $|p_i| \leq \phi_i \Leftrightarrow |-kp_i| \leq (k\phi_i)$, from equation (22)

$$\dot{p}_i + \left(\frac{\psi_i}{\phi_i}\right)p_i = (g(X)_{ii} - 1)u_i + f(X)_i + c_i(X,u,F) + m(X)_{ii}F_i \quad (24)$$

Thus let

$$\frac{\psi_i}{\phi_i} = k \quad \Rightarrow \quad \psi_i = (k\phi_i) \quad (25)$$

Hence equations (23), (24) and (25) give

$$\dot{\phi}_i + (k\phi_i) = (V(X)_{ii} - 1)|u_i| + \eta + U(X)_i + C_i(X,u,F) + W(X)_{ii}|F_i| \quad (26)$$

$$\dot{p}_i + kp_i = (g(X)_{ii} - 1)u_i + f(X)_i + c_i(X,u,F) + m(X)_{ii}F_i \quad (27)$$

Note that for a rigid environment k is very large (of the order of $10^7\ \mathrm{N\,m^{-1}}$) and hence equations (26) and (27) become approximately algebraic. So $k\phi_i$ and $-kp_i$ follow the RHS of equations (26) and (27) very closely. This, however, does not imply that there will be high control activity leading to control chattering, since by equation (25)

$$\psi_i \operatorname{sat}\frac{p_i}{\phi_i} \equiv -(k\phi_i)\operatorname{sat}\frac{(-kp_i)}{(k\phi_i)}$$

So, although ϕ_i was made very small due to k, p_i was made small by the *same* factor k [see equations (26) and (27)]. Thus the ratio p_i/ϕ_i remains unchanged and it is this fraction which is directly related to the control activity (Asada and Slotine 1986, p. 156). Again, from equations (26) and (27) one can see that $k\phi_i$ is a measure of the uncertainty in the model and $-kp_i$ is a measure of the perturbation between the nominal model and the actual physical system. Substituting (21) in (18) gives the following closed-loop contact dynamics

$$\ddot{\tilde{F}}_i + 2\lambda\dot{\tilde{F}}_i + \lambda^2\tilde{F}_i = -k\left[(1 - g(X)_{ii}^{-1})\ddot{x}_i + g(X)_{ii}^{-1}[f(X)_i + c_i(X,u,F) + m(X)_{ii}F_i] - \psi_i \operatorname{sat}\frac{p_i}{\phi_i}\right] \quad (28)$$

Summing up, equations (10), (11), (15), (16) and $\alpha(t) \equiv 0\ \forall t$ constitute the *trajectory tracking* control law for the dynamical system of equation (8), whereas equations (10), (11), (15), (16), (19), (21), (25) and (26) constitute the *force regulation* control law for the same dynamical system.

However, if one applies two different control laws (one for the non-contact phase and one for the contact phase) and switches between them when the system is entering or leaving contact, then it is difficult to ensure overall closed-loop system stability, especially at these switching instances. The system may enter a limit cycle with the manipulator oscillating to and fro between the two control laws when it crosses the boundary between contact and non-contact repeatedly at sufficiently high frequency. This situation may occur during impact with the environment due to the 'bouncing effect' caused by the coefficient of restitution of the environment. This limit cycling is caused by the fact that two different control laws are applied, and at these boundaries $u_{\text{contact}} \neq u_{\text{non-contact}}$, implying a discontinuity in the control law. The control law is discontinuous because $\alpha_i(t)$ is discontinuous [non-contact $\alpha_i(t) = 0$, whereas contact $\alpha_i(t)$ is given by equation (21)]. One might

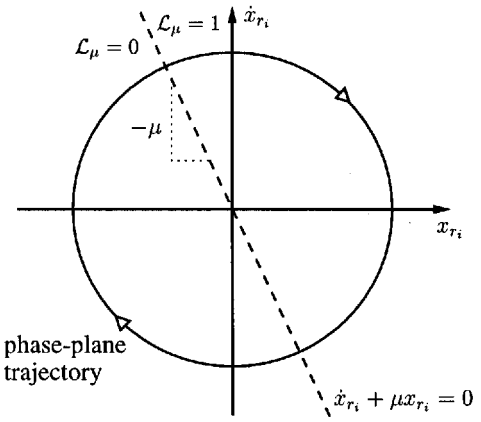

Figure 6. Gating signal $\mathcal{L}_\mu(x_{r_i}, \dot{r}_{r_i})$.

attempt to remove the discontinuity in $\alpha_i(t)$ by gating the RHS of (21) as follows

$$\ddot{\alpha}_i + 2\lambda\dot{\alpha}_i + \lambda^2\alpha_i = \left[\frac{\lambda^2 F_d}{k} + (\ddot{x}_{r_i} + 2\lambda\dot{x}_{r_i} + \lambda^2 x_{r_i}) - (V(X)_{ii}^{-1}\lambda\Phi_i)\ \text{sat}\ \frac{s_i}{\Phi_i} - (k\phi_i)\ \text{sat}\ \frac{(-kp_i)}{(k\phi_i)}\right]\mathcal{L}_\mu(x_{r_i}, \dot{x}_{r_i})$$

where $\mathcal{L}_\mu(x_{r_i}, \dot{x}_{r_i})$ is defined by $\mathcal{L}_\mu(x_{r_i}, \dot{x}_{r_i}) = 1$ if $\dot{x}_{r_i} + \mu x_{r_i} \geq 0$ and $\mathcal{L}_\mu(x_{r_i}, \dot{x}_{r_i}) = 0$ otherwise, as shown in figure 6. As x_{r_i} varies with time, it is moving in the $\dot{x}_{r_i}$–x_{r_i} plane and hence generating a gating signal $\mathcal{L}_\mu(x_{r_i}, \dot{x}_{r_i})$. Note that whenever $\mathcal{L}_\mu(x_{r_i}, \dot{x}_{r_i}) = 1$, the above equation reduces to (21), hence giving the force-regulating controller. Furthermore, when $\mathcal{L}_\mu(x_{r_i}, \dot{x}_{r_i}) = 0$, $\alpha(t)$ decays from any initial condition to zero and stays at zero thereafter, thus giving the trajectory-tracking controller.

The advantage of using this gating function is that the system changes from trajectory tracking to force regulation before actually hitting the environment, hence avoiding bouncing. This is desirable so that the system can slowly decrease its momentum and hit the environment with very small speed. Notice, from the definition of $\mathcal{L}_\mu(x_{r_i}, \dot{x}_{r_i})$, that the faster the system approaches the environment, the greater the distance allowed by this gating function to decelerate. The same reasoning applies when the manipulator is going from force control to trajectory-tracking control. Time (and hence its corresponding distance) is required to accelerate the system, which was initially at rest (at least in the constrained direction), to a speed equal to that of the reference trajectory.

The problem is, however, not yet solved as the above argument makes $\alpha_i(t)$ continuous but not $u_i(t)$. The reason for this is that the expression for $u_i(t)$ contains terms in $\dot{\alpha}_i(t)$ and $\ddot{\alpha}_i(t)$, and hence for $u_i(t)$ to be continuous $\alpha_i(t)$ must be twice differentiable everywhere. By low-pass filtering the gating signal $\mathcal{L}_\mu(x_{r_i}, \dot{x}_{r_i})$, continuity is obtained in $u_i(t)$. A first-order low-pass filter is considered not adequate as it is 'sluggish' in response. Thus, a second-order low-pass filter of the form $\omega_n^2/(\ell^2 + 2\xi\omega_n\ell + \omega_n^2)$ (where ℓ is the Laplace variable, so as not to confuse it with the sliding surfaces s) was considered. The design parameters ξ and ω_n can be found by optimization. Consequently, define $\mathcal{L}_\mu^{\xi,\omega_n}(x_{r_i}, \dot{x}_{r_i})$ as the low-pass filtered version of $\mathcal{L}_\mu(x_{r_i}, \dot{x}_{r_i})$ through $(\omega_n^2/(\ell^2 + 2\xi\omega_n\ell + \omega_n^2))$.

Thus, the resulting multivariable controller for the dynamical system described by (8), assuming known k, is given by

$$u_i = \ddot{x}_{d_i} - 2\lambda\dot{\tilde{x}}_i - \lambda^2\tilde{x}_i - (V(X)_{ii}^{-1}\lambda\Phi_i)\ \text{sat}\ \frac{s_i}{\Phi_i} \tag{29}$$

with

$$\tilde{x}_i = x_i - x_{d_i}, \quad x_{d_i} = x_{r_i} - \alpha_i \tag{30}$$

$$\dot{\Phi}_i + V(X)_{ii}^{-1+\text{sgn}\,\Phi_i}\lambda\Phi_i = V(X)_{ii}^{\text{sgn}\,\Phi_i}(V(X)_{ii} - 1)\left|\ddot{x}_{d_i} - 2\lambda\dot{\tilde{x}}_i - \lambda^2\tilde{x}_i\right| + V(X)_{ii}^{1+\text{sgn}\,\Phi_i}[\eta + U(X)_i + C_i(X, u, F) + W(X)_{ii}|F_i|] \tag{31}$$

$$\dot{\phi}_i + (k\phi_i) = \eta + U(X)_i + C_i(X, u, F) + W(X)_{ii}|F_i| + (V(X)_{ii} - 1)|u_i| \tag{32}$$

$$\ddot{\alpha}_i + 2\lambda\dot{\alpha}_i + \lambda^2\alpha_i = \left[\frac{\lambda^2 F_d}{k} + (\ddot{x}_{r_i} + 2\lambda\dot{x}_{r_i} + \lambda^2 x_{r_i}) - (V(X)_{ii}^{-1}\lambda\Phi_i)\ \text{sat}\ \frac{s_i}{\Phi_i} - (k\phi_i)\ \text{sat}\ \frac{(-kp_i)}{(k\phi_i)}\right]\mathcal{L}_\mu^{\xi,\omega_n}(x_{r_i}, \dot{x}_{r_i}) \tag{33}$$

$$s_i = \dot{\tilde{x}}_i + 2\lambda\tilde{x}_i + \lambda^2\int_o^t \tilde{x}_i\,dT - \dot{\tilde{x}}_i(0) - 2\lambda\tilde{x}_i(0) \tag{34}$$

$$(-kp_i) = \dot{\tilde{F}}_i + 2\lambda\tilde{F}_i + \lambda^2\int_o^t \tilde{F}_i\,dT - \dot{\tilde{F}}_i(0) - 2\lambda\tilde{F}_i(0) \tag{35}$$

In application, it is also necessary to modify equation (35) such that:

- integrator windup is avoided when the manipulator is in trajectory tracking mode. This is done by holding the integrator state constant when not in force control;
- the integrator is reset to zero and $\dot{\tilde{F}}_i(0)$, $\tilde{F}_i(0)$ are reset such that $(-kp_i) = 0$ every time the system enters force control mode; and

- a fictitious mathematical environment (with the same environment stiffness k as the actual physical environment) is mathematically constructed above the actual physical environment so that when the system changes from trajectory tracking to force regulation before actually hitting the physical environment, $-kp_i$ gives feedback according to this fictitious environment.

4.2. *Unknown environment stiffness*

The assumption that the environment stiffness k is known will now be relaxed and an adaptive algorithm will be derived to estimate this. Adaptation makes sense only when the system is in contact with the environment and is in force control. This is because force feedback is available only during this time, and it is this force feedback which provides information about the actual environment stiffness. During this time $\mathcal{L}_{\mu}^{\xi,\omega_n}(x_{r_i}, \dot{x}_{r_i}) = 1$ [see equation (33)]. The procedure adopted in this section to derive an adaptive observer uses the method of Canudas de Wit and Brogliato (1994), although the techniques used in this study are different from those presented there.

In practice k is unknown—only an estimate $\hat{k}$ is available. Consequently, since $\alpha_i(t)$ depends on k [see equation (33)], then only an estimate of $\alpha_i(t)$ is available. Denote this estimate by $\hat{\alpha}_i(t)$. If this estimate is used in the control law, then equation (29) becomes

$$u_i = (\ddot{x}_{r_i} - \ddot{\hat{\alpha}}_i) - 2\lambda[\dot{x}_i - (\dot{x}_{r_i} - \dot{\hat{\alpha}}_i)] - \lambda^2[x_i - (x_{r_i} - \hat{\alpha}_i)] - (V(X)_{ii}^{-1}\lambda\Phi_i)\ \mathrm{sat}\ \frac{s_i}{\Phi_i} \tag{36}$$

Substituting (36) in (9) and using the fact that $F_i = -kx_i$ results in

$$\ddot{F}_i + 2\lambda\dot{F}_i + \lambda^2 F_i = -k\Big[(\ddot{x}_{r_i} + 2\lambda\dot{x}_{r_i} + \lambda^2 x_{r_i}) - (\ddot{\hat{\alpha}}_i + 2\lambda\dot{\hat{\alpha}}_i + \lambda^2\hat{\alpha}_i) + (1 - g(X)_{ii}^{-1})\ddot{x}_i + g(X)_{ii}^{-1}[f(X)_i + c_i(X, u, F) + m(X)_{ii}F_i] - (V(X)_{ii}^{-1}\lambda\Phi_i)\ \mathrm{sat}\ \frac{s_i}{\Phi_i}\Big] \tag{37}$$

Now, using equation (33) in (37) gives

$$\ddot{\tilde{F}}_i + 2\lambda\dot{\tilde{F}}_i + \lambda^2\tilde{F}_i = k\Big[(\ddot{\tilde{\alpha}}_i + 2\lambda\dot{\tilde{\alpha}}_i + \lambda^2\tilde{\alpha}_i) - (1 - g(X)_{ii}^{-1})\ddot{x}_i - g(X)_{ii}^{-1}[f(X)_i + c_i(X, u, F) + m(X)_{ii}F_i] - (k\phi_i)\ \mathrm{sat}\ \frac{(-kp_i)}{(k\phi_i)}\Big] \tag{38}$$

where $\tilde{\alpha}_i = \hat{\alpha}_i - \alpha_i$. Equation (38) represents the closed-loop contact error dynamics. The terms in the RHS are due to the uncertainty. Also, equation (33) can be parametrized as follows

$$\ddot{\alpha}_i + 2\lambda\dot{\alpha}_i + \lambda^2\alpha_i = \theta\Omega + (\ddot{x}_{r_i} + 2\lambda\dot{x}_{r_i} + \lambda^2 x_{r_i}) - (V(X)_{ii}^{-1}\lambda\Phi_i)\ \mathrm{sat}\ \frac{s_i}{\Phi_i} - (k\phi_i)\ \mathrm{sat}\ \frac{(-kp_i)}{(k\phi_i)} \tag{39}$$

where $\theta = 1/k$ and $\Omega = \lambda^2 F_d$. Note that k is taken to be independent of i, thus implying one adaptation law. Equation (39) can be used as a basis for the design of an adaptive observer for $\theta = 1/k$. Again, let the Laplace complex variable be denoted by ℓ and define $\hat{\theta} = 1/\hat{k}$.

Then consider the system described by equation (8), together with the control law given by equation (36) and the following adaptive observer structure

$$\ddot{\hat{\alpha}}_i + 2\lambda\dot{\hat{\alpha}}_i + \lambda^2\hat{\alpha}_i = [\hat{\theta}\Omega + \dot{\hat{\theta}}\bar{\Omega}_i] + (\ddot{x}_{r_i} + 2\lambda\dot{x}_{r_i} + \lambda^2 x_{r_i}) - (V(X)_{ii}^{-1}\lambda\Phi_i)\ \mathrm{sat}\ \frac{s_i}{\Phi_i} - (\hat{k}\phi_i)\ \mathrm{sat}\ \frac{(-\hat{k}p_i)}{(\hat{k}\phi_i)} \tag{40}$$

with

$$\ddot{\bar{\Omega}}_i + \rho\dot{\bar{\Omega}}_i = \Omega, \qquad 0 < \rho < 2\lambda \tag{41}$$

$$\dot{\hat{\theta}} = -\gamma\bar{\Omega}_i\tilde{F}_i, \qquad \gamma > 0 \tag{42}$$

Now, a Lyapunov-type argument will be used to justify that such an observer results in $\hat{\theta} \to \theta$ (i.e. $\hat{k} \to k$) and $\tilde{F}_i \to 0$ as $t \to \infty$. Subtracting (39) from (40) gives

$$\ddot{\tilde{\alpha}}_i + 2\lambda\dot{\tilde{\alpha}}_i + \lambda^2\tilde{\alpha}_i = [\hat{\theta}\Omega + \dot{\hat{\theta}}\bar{\Omega}_i - \theta\Omega] - (\hat{k}\phi_i)\ \mathrm{sat}\ \frac{(-\hat{k}p_i)}{(\hat{k}\phi_i)} + (k\phi_i)\ \mathrm{sat}\ \frac{(-kp_i)}{(k\phi_i)}$$

Introducing $\tilde{\theta} = \hat{\theta} - \theta$, noting that $\dot{\tilde{\theta}} = \dot{\hat{\theta}}$ since θ is constant and using equation (41) results in

$$\ddot{\tilde{\alpha}}_i + 2\lambda\dot{\tilde{\alpha}}_i + \lambda^2\tilde{\alpha}_i = \left(\frac{\mathrm{d}}{\mathrm{d}t} + \rho\right)[\tilde{\theta}\bar{\Omega}_i] - (\hat{k}\phi_i)\,\mathrm{sat}\,\frac{(-\hat{k}p_i)}{(\hat{k}\phi_i)} + (k\phi_i)\,\mathrm{sat}\,\frac{(-kp_i)}{(k\phi_i)} \quad (43)$$

Using equation (43) in (38) yields

$$\ddot{\tilde{F}}_i + 2\lambda\dot{\tilde{F}}_i + \lambda^2\tilde{F}_i = k\left[\left(\frac{\mathrm{d}}{\mathrm{d}t} + \rho\right)[\tilde{\theta}\bar{\Omega}_i] - g(X)_{ii}^{-1}[f(X)_i + c_i(X,u,F) + m(X)_{ii}F_i] - (1 - g(X)_{ii}^{-1})\ddot{x}_i - (\hat{k}\phi_i)\,\mathrm{sat}\,\frac{(-\hat{k}p_i)}{(\hat{k}\phi_i)}\right]$$

Taking the Laplace transform $\mathscr{L}$ in turn gives

$$\tilde{F}_i(\ell) = k\frac{(\ell + \rho)}{(\ell^2 + 2\lambda\ell + \lambda^2)}\mathscr{L}\{\tilde{\theta}\bar{\Omega}_i\} - \frac{k}{(\ell^2 + 2\lambda\ell + \lambda^2)}\mathscr{L}\left\{(1 - g(X)_{ii}^{-1})\ddot{x}_i + g(X)_{ii}^{-1}[f(X)_i + c_i(X,u,F) + m(X)_{ii}F_i] + (\hat{k}\phi_i)\,\mathrm{sat}\frac{(-\hat{k}p_i)}{(\hat{k}\phi_i)}\right\}$$

The second input will be approximately equal to zero, since $(-\hat{k}p_i)$ is varying so as to cancel out the effects of the other terms.† It will in fact be exactly zero in the absence of uncertainty and will otherwise be very small. Defining $W(\ell) = k(\ell + \rho)/(\ell^2 + 2\lambda\ell + \lambda^2)$ thus gives

$$\tilde{F}_i(\ell) \approx W(\ell)\mathscr{L}\{\tilde{\theta}\bar{\Omega}_i\} \quad (44)$$

Now let $W(\ell)$ have a state-space representation of the form

$$\left[\begin{array}{c|c} A & b \\ \hline c^{\mathrm{T}} & 0 \end{array}\right]$$

where A is Hurwitz. Then equation (44) gives

$$\dot{\sigma} = A\sigma + b[\tilde{\theta}\bar{\Omega}_i] \quad (45)$$

$$\tilde{F}_i = c^{\mathrm{T}}\sigma \quad (46)$$

where σ is the state vector. Since $W(\ell)$ is *strictly positive real* whenever $\rho < 2\lambda$ (Lanzon 1997), then the Kalman–Yakubovich–Popov lemma (Lefschetz 1965) states that

$$\exists\, P > 0, Q > 0: \quad A^{\mathrm{T}}P + PA = -Q \quad (47)$$

$$b^{\mathrm{T}}P = c^{\mathrm{T}} \quad (48)$$

Then, choosing $V = \sigma^{\mathrm{T}}P\sigma + \tilde{\theta}^2/\gamma$ as the Lyapunov candidate function, differentiating it and using equations (42), (45)–(48) yields

$$\dot{V} = \dot{\sigma}^{\mathrm{T}}P\sigma + \sigma^{\mathrm{T}}P\dot{\sigma} + 2\tilde{\theta}\frac{\dot{\tilde{\theta}}}{\gamma}$$

$$\dot{V} = \left[A\sigma + b[\tilde{\theta}\bar{\Omega}_i]\right]^{\mathrm{T}}P\sigma + \sigma^{\mathrm{T}}P\left[A\sigma + b[\tilde{\theta}\bar{\Omega}_i]\right] + 2\tilde{\theta}\frac{\dot{\hat{\theta}}}{\gamma}$$

$$\dot{V} = \sigma^{\mathrm{T}}(A^{\mathrm{T}}P + PA)\sigma + 2\tilde{\theta}\bar{\Omega}_i b^{\mathrm{T}}P\sigma + 2\tilde{\theta}\frac{\dot{\hat{\theta}}}{\gamma}$$

$$\dot{V} = -\sigma^{\mathrm{T}}Q\sigma + 2\tilde{\theta}\left[\bar{\Omega}_i\tilde{F}_i + \frac{\dot{\hat{\theta}}}{\gamma}\right]$$

$$\dot{V} = -\sigma^{\mathrm{T}}Q\sigma < 0 \quad \forall\sigma \neq 0$$

Now, since $\dot{V} < 0\ \forall\sigma \neq 0$, then equations (45) and (46) imply that $\hat{\theta} \to \theta$ and $\tilde{F}_i \to 0$ as $t \to \infty$. This is an algorithm justification, rather than a proof, since convergence is based on the approximation $\tilde{F}_i(\ell) \approx W(\ell)\mathscr{L}\{\tilde{\theta}\bar{\Omega}_i\}$.

Summing up, the resulting adaptive sliding-mode controller is given by combining equations (29)–(35) and the adaptive observer given by equations (40)–(42). The complete control law is thus given by

$$u_i = \ddot{x}_{\mathrm{d}_i} - 2\lambda\dot{\tilde{x}}_i - \lambda^2\tilde{x}_i - (V(X)_{ii}^{-1}\lambda\Phi_i)\,\mathrm{sat}\,\frac{s_i}{\Phi_i} \quad (49)$$

with

$$\tilde{x}_i = x_i - x_{\mathrm{d}_i}, \qquad x_{\mathrm{d}_i} = x_{\mathrm{r}_i} - \hat{\alpha}_i \quad (50)$$

$$\dot{\Phi}_i + V(X)_{ii}^{-1+\,\mathrm{sgn}\,\Phi_i}\lambda\Phi_i = V(X)_{ii}^{\mathrm{sgn}\,\Phi_i}(V(X)_{ii} - 1)\left|\ddot{x}_{\mathrm{d}_i} - 2\lambda\dot{\tilde{x}}_i - \lambda^2\tilde{x}_i\right| + V(X)_{ii}^{1+\,\mathrm{sgn}\,\Phi_i}[\eta + U(X)_i + C_i(X,u,F) + W(X)_{ii}|F_i|] \quad (51)$$

$$\dot{\phi}_i + (\hat{k}\phi_i) = \eta + U(X)_i + C_i(X,u,F) + W(X)_{ii}|F_i| + (V(X)_{ii} - 1)|u_i| \quad (52)$$

$$\ddot{\hat{\alpha}}_i + 2\lambda\dot{\hat{\alpha}}_i + \lambda^2\hat{\alpha}_i = \left[[\hat{\theta}\Omega + \dot{\hat{\theta}}\bar{\Omega}_i] + (\ddot{x}_{\mathrm{r}_i} + 2\lambda\dot{x}_{\mathrm{r}_i} + \lambda^2 x_{\mathrm{r}_i}) - (V(X)_{ii}^{-1}\lambda\Phi_i)\,\mathrm{sat}\,\frac{s_i}{\Phi_i} - (\hat{k}\phi_i)\,\mathrm{sat}\,\frac{(-\hat{k}p_i)}{(\hat{k}\phi_i)}\right]\mathcal{L}_{\mu}^{\xi,\omega_n}(x_{\mathrm{r}_i}, \dot{x}_{\mathrm{r}_i}) \quad (53)$$

† This can be seen, after some algebra, by eliminating u_i from equations (9) and (27).

$$\dot{\bar{\Omega}}_i + \rho\bar{\Omega}_i = \Omega, \quad 0 < \rho < 2\lambda, \quad \Omega = \lambda^2 F_d \tag{54}$$

$$\dot{\hat{\theta}} = -\gamma\bar{\Omega}_i\tilde{F}_i, \qquad \gamma > 0, \qquad \hat{k} = \frac{1}{\hat{\theta}} \tag{55}$$

$$s_i = \dot{\tilde{x}}_i + 2\lambda\tilde{x}_i + \lambda^2\int_o^t \tilde{x}_i\,dT - \dot{\tilde{x}}_i(0) - 2\lambda\tilde{x}_i(0) \tag{56}$$

$$(-\hat{k}p_i) = \dot{\tilde{F}}_i + 2\lambda\tilde{F}_i + \lambda^2\int_o^t \tilde{F}_i\,dT - \dot{\tilde{F}}_i(0) - 2\lambda\tilde{F}_i(0) \tag{57}$$

In application, the same modifications as previously described at the end of § 4.1 should be performed on equation (57). Recall also that adaptation is only sensible when the system is in contact with the environment and is in force control. Thus equations (54) and (55) are used only in this situation. Note that since k was taken as the same for all i, then there is only one adaptation law above.

5. Simulation results

The above control law was applied to a planar two-degree of freedom manipulator and the system behaviour was simulated using SIMULINK 2.0. The robot parameters are as follows: Link 1 is 300 mm long and weighs 484 g, whereas Link 2 is 270 mm long and weighs 260 g. The robot model used in the simulation was a 'lumped' parameter model. Model uncertainty was described by smooth vector and matrix-valued functions f, G and M of the state-vector X. The following results were obtained.

Figure 7 shows a portrait of the reference and controlled-output trajectories. The environment is at $x_1 \geq 0$ and $x_2 \geq 0$. The end-effector follows the reference trajectory x_r when unconstrained but stays at the surface of the environment, regulating force, when the reference

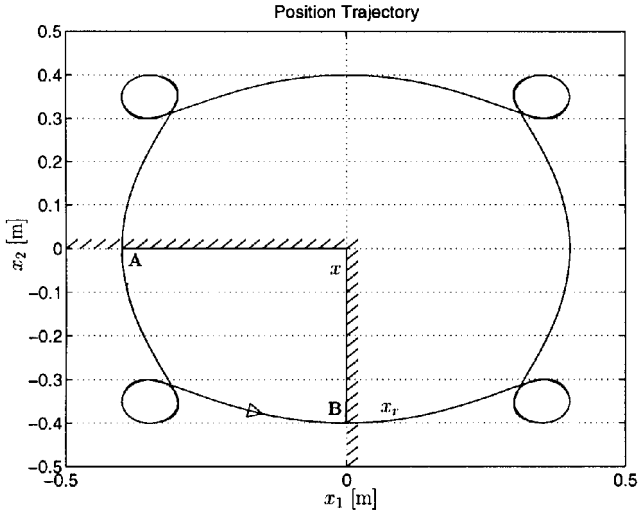

Figure 7. Trajectory portrait.

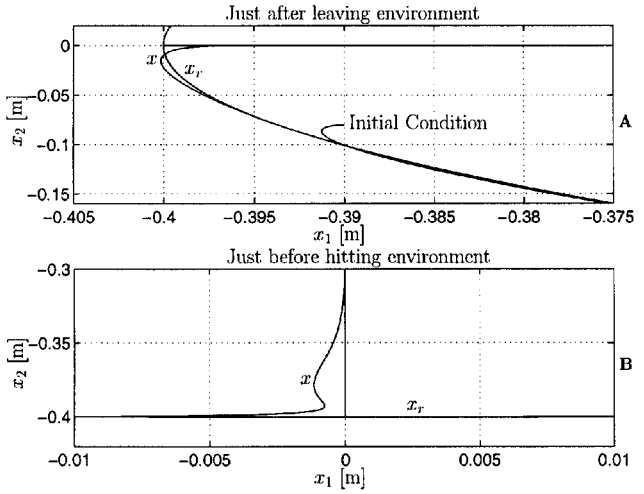

Figure 8. Trajectory portrait magnification.

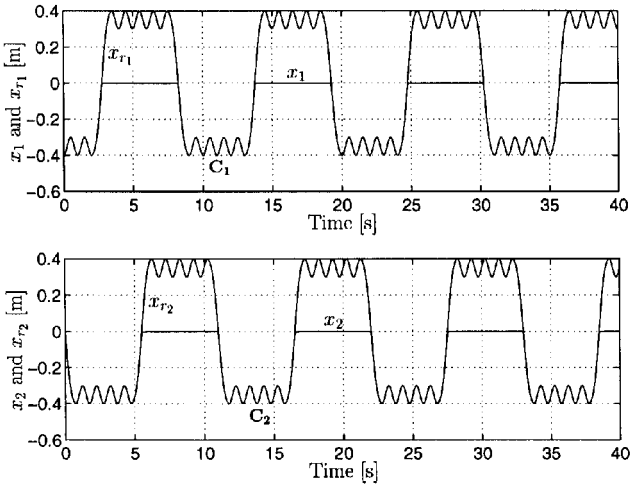

Figure 9. Position trajectories.

trajectory goes inside the environment. Thus, the manipulator regulates force in the constrained direction and tracks the reference trajectory in the remaining unconstrained direction. Figure 8 is a magnification of figure 7 just after leaving the environment and just before hitting the environment. The initial condition is also shown in figure 8.

The reference position x_{r_i} and the controlled-output position x_i are also shown against time in figure 9. Note that $x_{r_i} \geq 0$ means inside the environment whilst $x_{r_i} < 0$ means outside the environment. This peculiar reference trajectory was chosen because it has characteristics which test the controller's trajectory-tracking and force-regulation capabilities. This reference trajectory is made up from three parts. The first part is a sine-wave varying outside the environment. This tests the trajectory-tracking performance. The second part is a spline which was designed, for ease of use, to have exactly $1\,\mathrm{m\,s^{-1}}$ velocity

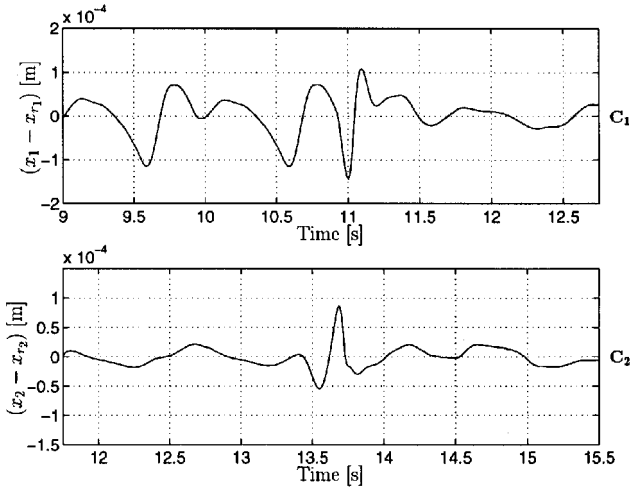

Figure 10. Trajectory tracking position-errors.

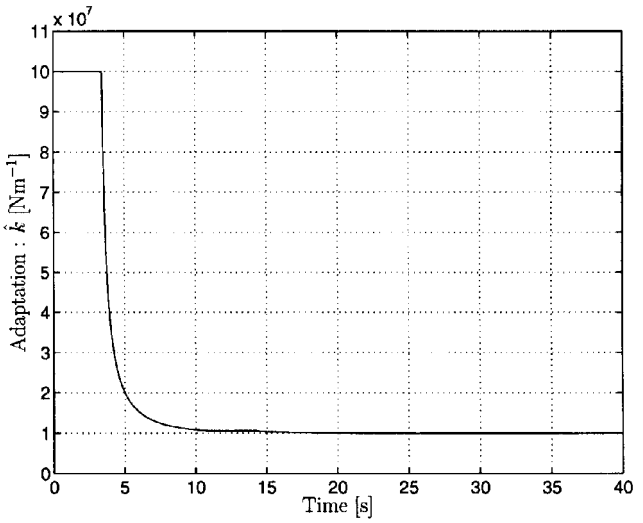

Figure 11. Environment stiffness adaptation.

at the moment of crossing $x_{r_i} = 0$. This assesses the behaviour of the controller at the moment of impact and just after the end-effector leaves the environment. The third part composing this reference trajectory is again a sine-wave, but this time varying inside the environment. This enables the force-regulation performance to be tested. Note that an inherent assumption throughout the controller synthesis was that x_{r_i} is twice differentiable. This assumption is quite mild and can easily be satisfied in practice. The trajectory tracking error is depicted in figure 10. It is of the order of 10^{-4} m. The two subplots in this figure are on a different time-scale because the corresponding reference trajectories, in the individual directions, are phase-shifted from each other. Hence trajectory motion control occurs at different times for the two individual directions.

The adaptive algorithm's estimate $\hat{k}$ is given in figure 11. When the end-effector is not in contact with

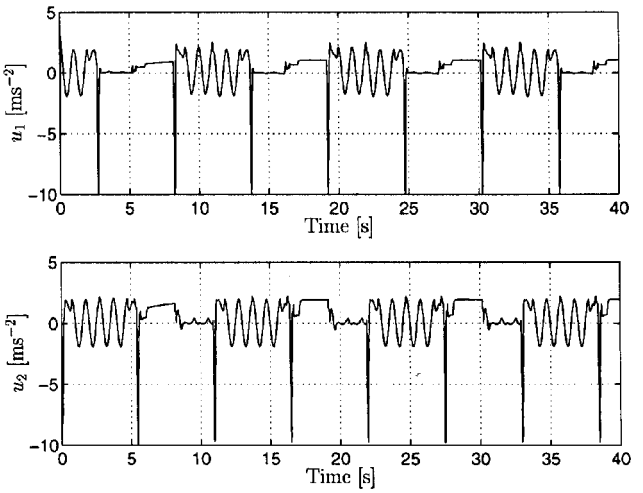

Figure 12. Control inputs.

either surface, adaptation stops and this results in the horizontal lines seen in figure 11 (i.e. $\hat{k}$ is not updated when not in contact). Note that $\hat{k}$ converges to k in about 25 s. A point which needs to be made here is that the adaptation gain γ was chosen small enough so that adaptation is slow when compared to the normal system dynamics. This was required to ensure two different time-scales in design (Åström and Wittenmark 1989)—that is, to ensure that the controller can be first designed by assuming that the environment stiffness k is completely known and then relaxing this assumption by adaptively estimating k for that controller.

The control input u_i is illustrated in figure 12. Note that, due to the cross-coupling terms, each control input is affected by the other control input. The negative spikes are due to the fact that when the manipulator is approaching the environment it must undergo rapid deceleration and when it is leaving the environment (after force control) it must be accelerated very quickly in the negative x_i-direction.

The desired trajectory $x_{d_i}(t)$ is given in figure 13 together with its magnification during force control in figure 14. The reaction forces exerted by the environment on the end-effector are shown in figure 15 and a magnification of the error between the actual force and the desired contact force is given in figure 16. It is worth noting that the overshoot in force during simulation is less than 0.5%. It is also interesting to analyse the cause of the variations from the nominal curves in figures 14 and 16. From these figures, it can be seen that if model uncertainty or disturbances cause the contact force to 'increase negatively' more than the nominal curve (i.e. pushing more than necessary into the environment), then x_{d_i} will vary (due to a variation in α_i) so as to pull the manipulator from pushing further into the environment (i.e. x_{d_i} goes negative). If, on the other

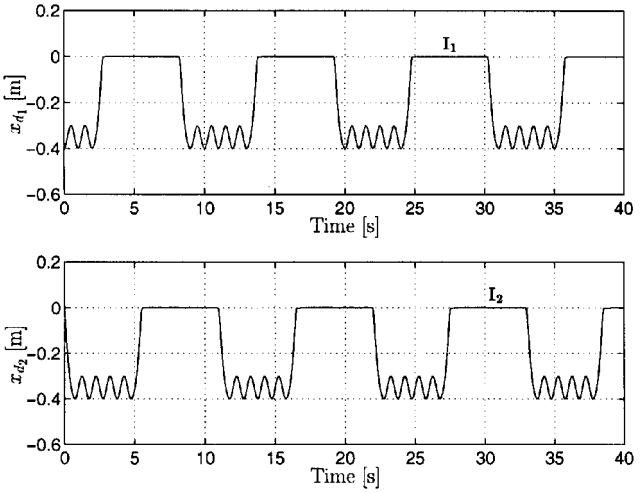

Figure 13. Desired trajectories.

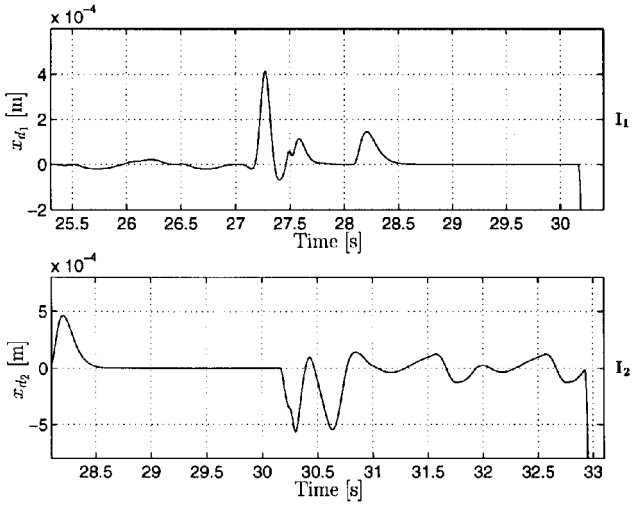

Figure 14. Desired trajectory magnification.

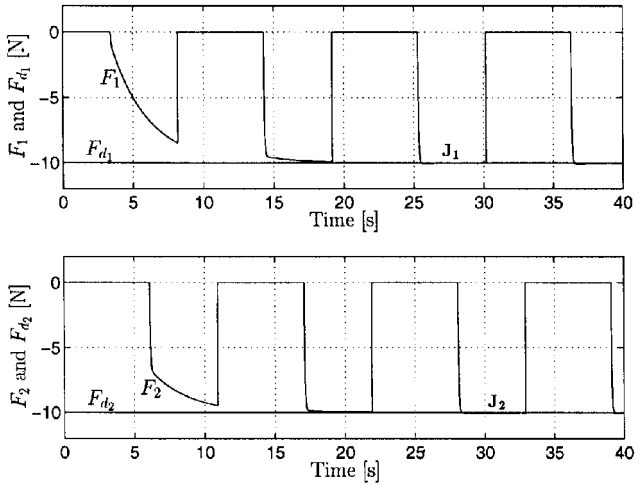

Figure 15. Reaction forces.

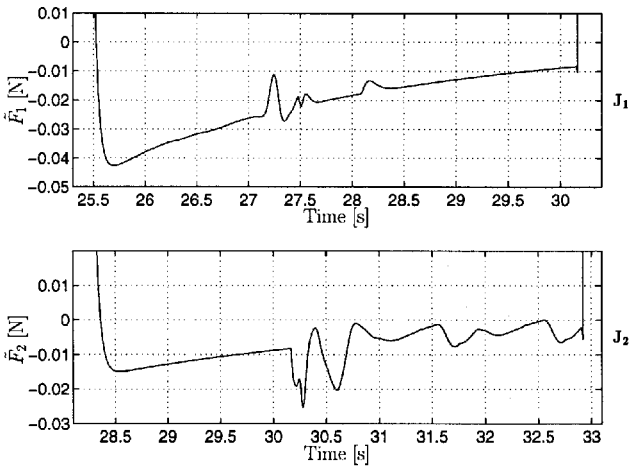

Figure 16. Magnification of reaction forces.

hand, disturbances or model uncertainty cause the manipulator to push less than desired on the environment (i.e. F_i starts increasing), then x_{d_i} will vary (due to a variation in α_i) so as to make the manipulator push more into the environment (i.e. x_{d_i} goes largely positive to counteract this uncertainty).

Robustness against small changes in environment location was also investigated. It was found that such changes cause minor variations in the results depicted below. Only the time taken by the adaptive algorithm to make the estimate $\hat{k}$ converge to the actual value k increases.

6. Physical implementation

The complete multivariable adaptive sliding-mode control law derived in § 4 was implemented on a planar 2-degree of freedom robot arm.

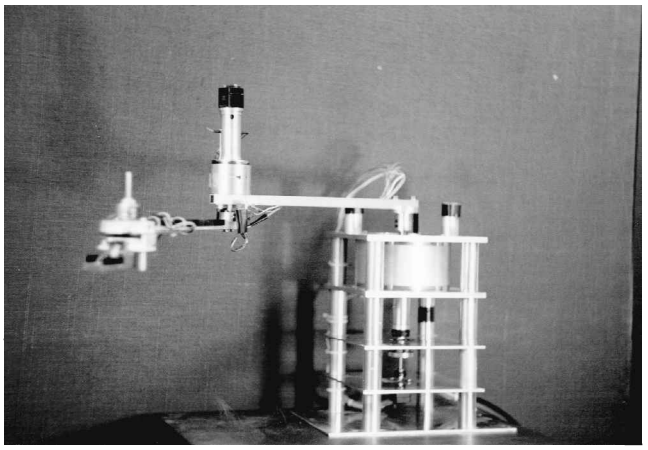

Figure 17. Planar 2-degree of freedom manipulator.

Figure 18. End-effector and environment.

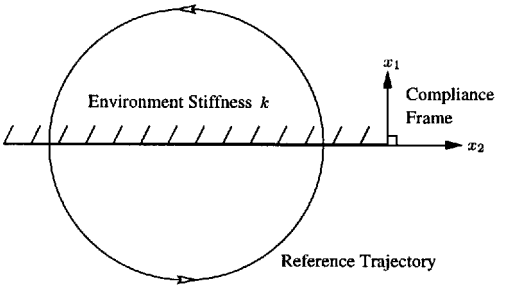

Figure 19. Compliance frame, reference trajectory and environment.

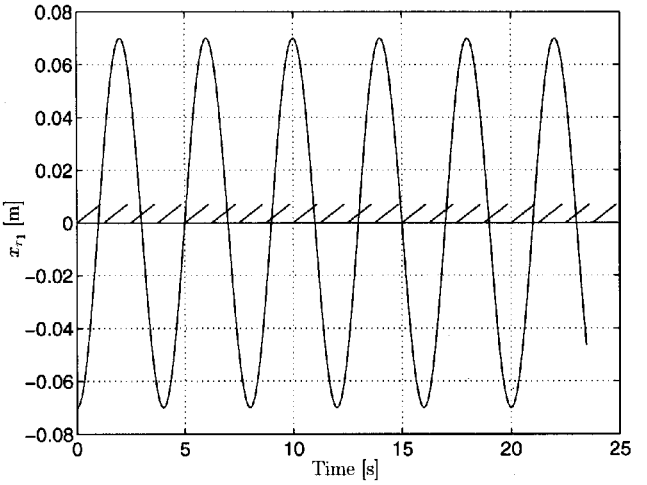

Figure 20. End-effector reference position x_{r_1}.

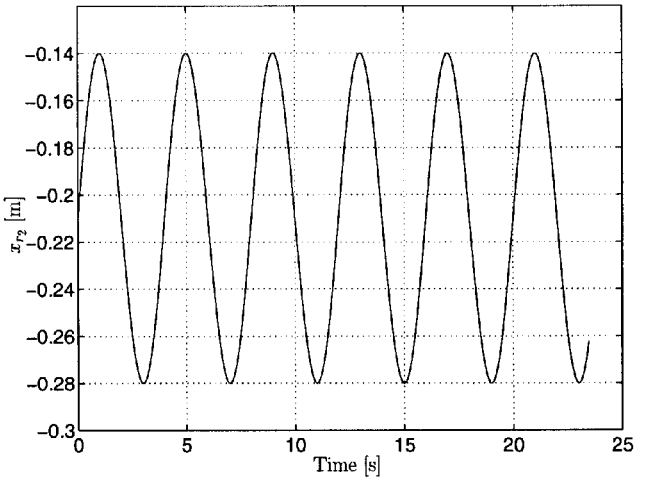

Figure 21. End-effector reference position x_{r_2}.

6.1. *Experimental equipment*

The arm shown in figure 17 exhibits most of the non-linear and coupling effects which are present in multi-link robots, and hence was considered suitable to test the effectiveness of the controller. This arm is equipped with two dc motors, one at each joint. Link 1 is 300 mm long and weighs 484 g. Link 2 is 270 mm long and weighs 260 g. At each joint, there is a potentiometer and a tacho-generator which measure the link angular position and velocity respectively. The environment (i.e. contact surface) was made out of Perspex and strain gauges were mounted behind it to give contact force feedback. The force sensor was mounted behind the environment rather than on the end-effector, for ease of construction. The compound environment stiffness is unknown (and need not be known since the adaptive algorithm estimates it) but is of the order of $10^4\,\mathrm{N\,m^{-1}}$. The interaction of the robot end-effector with the environment is illustrated in figure 18. The control law was coded in Borland Pascal 7 and was run on a 486 PC with 120 MHz CPU clock speed. The sampling rate was 250 Hz—much more than is actually required.

6.2. *Experimental results*

The experimental results are shown in figures 20–27. For simplicity, the nominal model used to describe the robot dynamics was chosen to be a *lumped* model. That is, the link mass was assumed to be a point mass concentrated at the end—hence the centre of gravity of the link is also at the end and the moment of inertia about this point is zero. In reality, the link mass is distributed, thus giving a centre of gravity which is not exactly at the end of the link and a moment of inertia about this point which is non-zero. The results in this section show that, even with such a crude nominal model, the manipulator is controlled to an acceptable level of performance.

In the experimental results, x_{r_i} and x_i denote the end-effector reference position and end-effector actual position respectively, read with respect to the compliance frame. Also, τ_i denotes the joint torques exerted by the dc motors on their respective links, and F_1 denotes the reaction force exerted by the environment on robot end-effector. The desired contact force was set to -3 N.

The task-space reference trajectories used in the experiments were simple sine-waves in each coordinate

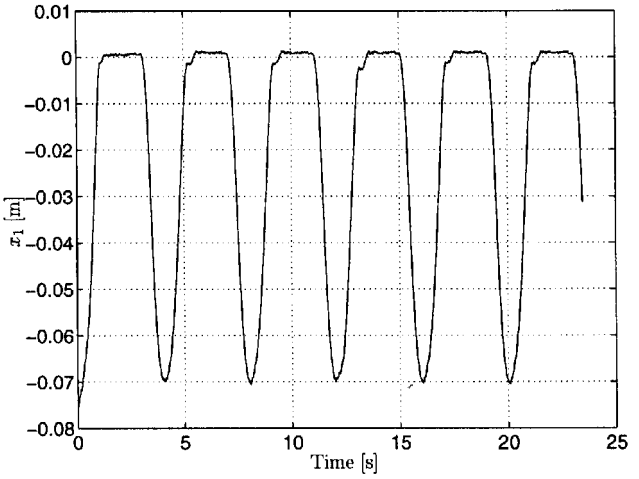

Figure 22. End-effector actual postion x_1.

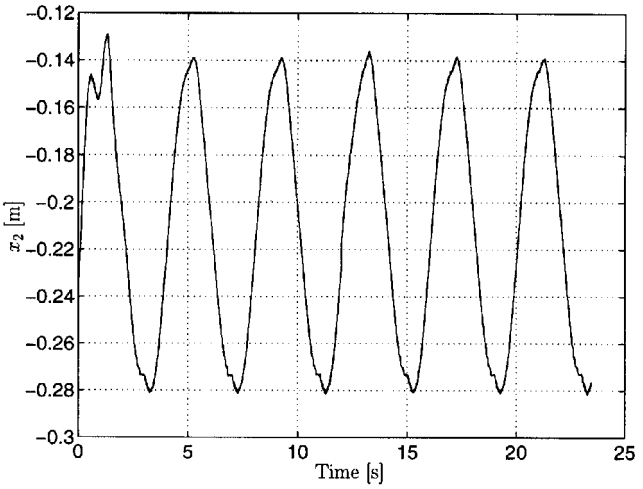

Figure 23. End-effector actual position x_2.

direction, to simplify programming. These are shown in figures 20 and 21. The resulting circular trajectory is depicted in figure 19. Its radius is 7 cm and its diameter lies along the environment surface. Thus, the end-effector is required to follow the semicircle which lies outside the environment and slide along the surface, regulating force, when the reference trajectory is tracing the remaining semicircle which goes deep inside the environment. The end-effector location, in each coordinate direction, is shown in figures 22 and 23. The resulting end-effector motion in the x_1–x_2 plane is given in figure 24. The raggedness in this curve is probably due to stiction, lack of control action between the sampling instances and the general lightweight construction of the robot arm. In figure 22, there is a 'kink' in the curve as it approaches $x_1 = 0$ (i.e. the environment). This is because the manipulator starts decreasing its end-effector velocity as it approaches the environment, so that it hits the environment with small momentum.

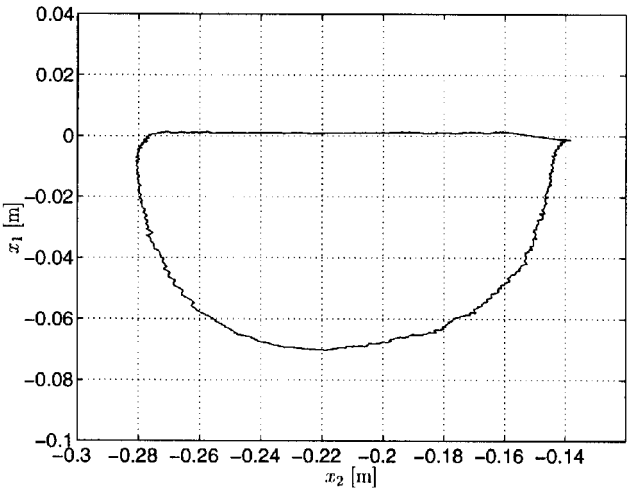

Figure 24. End-effector motion in x_1–x_2 plane.

Figures 25 and 26 show the corresponding joint torques τ_i obtained from u_i through the use of the partial feedback linearization control law. These output signals are noisy because of the noise in the force measurement and quantization errors in the A/D conversion.

Figure 27 clearly shows the effects of adaptation. The overshoot in force caused by the end-effector hitting the environment was reasonably large in the experiments. The main reason for this is the *delay* before the controller starts reacting to the force signal. This delay is caused by two major sources. The inertia of the environment acts like a low-pass filter which stores the kinetic energy transmitted to it during impact. Since the strain gauges are mounted behind the environment, they detect a force change only after the environment has moved. Putting the force sensor on the end-effector would considerably reduce this effect. The second effect is due to the delay caused by the fact that each signal is sampled (at 4 ms) and hence corrective control action is given only at these sampling instances. Errors in regulating the force at the desired value of − 3 N result from unrepeatability in the strain gauge measurements† and unmodelled dynamics which are not covered by the uncertainty structure used. The latter can be reduced by working out a closer nominal model to the actual physical system, instead of using a very crude nominal model. The oscillation in the force signal after the manipulator leaves the environment is again caused by the fact that the force sensor is placed behind the environment which swings slightly after the manipulator loses contact.

Consequently, the largest problems in the experiments were caused by the fact that the force sensor

† The application of a force of − 3 N twenty times gave variations in force measurement up to ±10%.

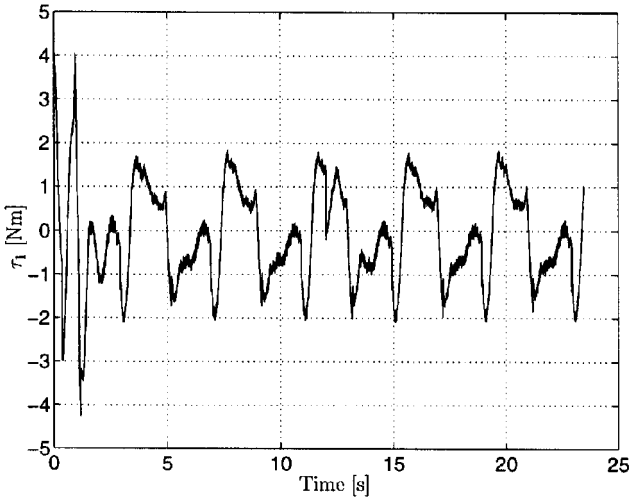

Figure 25. Joint 1 torque.

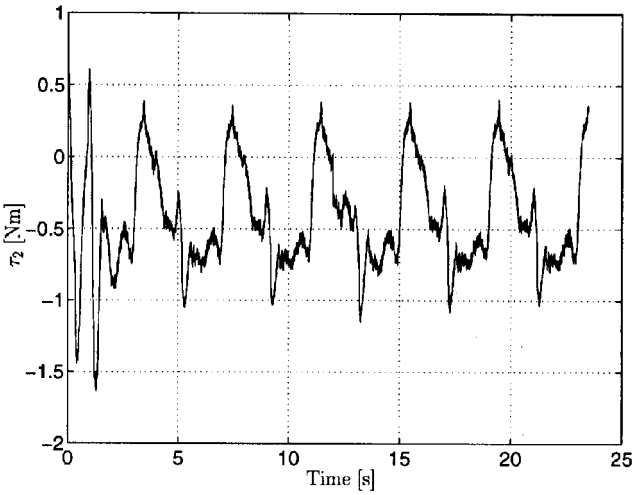

Figure 26. Joint 2 torque.

was placed behind the environment. The above experimental results can thus be improved by mounting the force sensor on the end-effector instead.

Robustness against small changes in environment location was also investigated. As in the simulations, small changes in environment location gave minor variations in the experimental results. The only difference is the fact that the adaptive algorithm takes more time to converge to the actual value.

7. Conclusions

A *single* control law has been derived to control the manipulator during both the trajectory-tracking and the force-regulating phases by introducing the continuous variable $\alpha(t)$. Having a single control law is desirable because it is easier to ensure stability of the closed-loop system throughout the entire operational space. This is

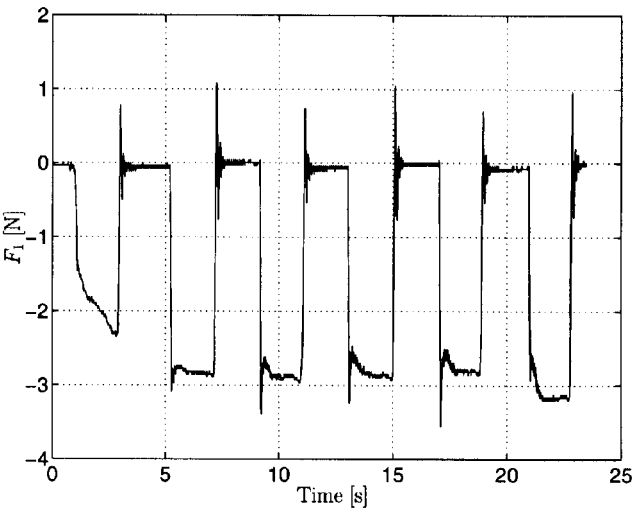

Figure 27. Reaction force.

preferable to designing separate controllers for the trajectory-tracking phase and the force-regulating phase, and then switching between the two controllers (or interpolating between the two control laws) when the system changes constraints. The 'price' paid for using only one control law is increased controller complexity. The controller derived here is made up from $10n$ equations, where n is the number of degrees of freedom of the manipulator; whereas controllers designed only for trajectory tracking or force regulation would be described by far fewer equations.

Furthermore, an adaptive observer, which is an extension of the ideas presented by Canudas de Wit and Brogliato (1994), was derived to estimate the unknown environment stiffness. Their ideas were extended to a multiple-input multiple-output non-linear system with uncertain dynamics, and the control law derived here is valid during both the contact and non-contact phases. The resulting observer structure is quite different because sliding-mode control has been used here to take care of the uncertain dynamics.

The experimental element of this paper demonstrates the applicability of the controller, although further work could improve and extend the results presented here. Moreover, the general compliant motion control problem requires a solution where the environment location/geometry is unknown and is, in general, non-stationary.

Acknowledgments

The first author's research is financially supported by a Cambridge Commonwealth Trust Scholarship, a Control Group Grant, a Meek Scholarship, a W. G. Collins Award and a C. T. Taylor Studentship—all from the University of Cambridge. These are all gratefully acknowledged.

References

An, C. H., and Hollerbach, J. M., 1987, Kinematic stability issues in force control of manipulators. In *IEEE International Conference on Robotics and Automation*, pages 897–903, Raleigh, NC, USA.

Asada, H., and Slotine, J.-J. E., 1986, *Robot Analysis and Control*. John Wiley and Sons, Inc.

Åström, K. J., and Wittenmark, B., 1989, *Adaptive Control*. Addison-Wesley Publishing Company, Inc.

Canudas de Wit, C., and Brogliato, B., 1994, Direct adaptive impedance control. In L. Sciavicco, C. Bonivento and F. Nicolò (Eds), *Preprints of the Fourth IFAC Symposium on Robot Control*, Capri, Italy, Vol. 2, pp. 395–400.

Chiaverini, S., and Sciavicco, L., 1993, The parallel approach to force/position control of robotic manipulators. *IEEE Transactions on Robotics and Automation*, **9**, 361–373.

Chiaverini, S., Siciliano, B., and Villani, L., 1998, Force and position tracking: Parallel control with stiffness adaptation. *IEEE Control Systems*, 27–33.

Colbaugh, R., Seraji, H., and Glass, K., 1995, Adaptive compliant motion control for dexterous manipulators. *International Journal of Robotics Research*, **14**, 270–280.

Fisher, W. D., and Mujtaba, M. S., 1992, Hybrid position/force control: a correct formulation. *International Journal of Robotics Research*, **11**, 299–311.

Hogan, N., 1984, Impedance control of industrial robots. *Robotics and Computer Integrated Manufacturing*, **1**, 97–113.

Kwan, C. M., 1995, Hybrid force/position control for manipulators with motor dynamics using a sliding–adaptive approach. *IEEE Transactions on Automatic Control*, **40**, 963–968.

Lanzon, A., 1997, Compliant motion control for robotic manipulators. Master's thesis, University of Cambridge, Department of Engineering, Cambridge, UK.

Lefschetz, S., 1965, *Stability of Nonlinear Control Systems* (New York: Academic Press) pp. 114–118.

Lipkin, H., and Duffy, J., 1986, Invariant kinestatic filtering. In *Preprints of 6th CISM–IFToMM Symposium on Theory and Practice of Robots and Manipulators*, Cracow, Poland, pp. 96–103.

Lu, Z., and Goldenberg, A. A., 1995, Robust impedance control and force regulation: Theory and experiments. *International Journal of Robotics Research*, **14**, 225–254.

Luh, J. Y. S., Walker, M. W., and Paul, R. P., 1980, Resolved acceleration control of mechanical manipulators. *IEEE Transactions on Automatic Control*, **AC-25**, 468–567.

Mason, M. T., 1981, Compliance and force control for computer controlled manipulators. *IEEE Transactions on Systems, Man and Cybernetics*, **SMC-11**, 418–432.

Murrary, R. M., Li, Z., and Sastry, S. S., 1994, *A Mathematical Introduction to Robotic Manipulation* (CRC Press).

Paul, R. P., and Shimano, B., 1982, Compliance and control. In M. Brady *et al.* (Eds), *Robot Motion Planning and Control* (Cambridge, MA: MIT Press), pp. 404–418.

Raibert, M. H., and Craig, J. J., 1981, Hybrid prosition/force control of manipulators. *ASME Journal of Dynamic Systems, Measurement and Control*, **102**, 126–133.

Salisbury, K., 1980, Active stiffness control of a manipulator in cartesian coordinates. In *Proceedings of the 19th IEEE Conference on Decision and Control*, Albuquerque, NM, pp. 87–97.

Seraji, H., 1998, Nonlinear and adaptive control of force and compliance in manipulators. *International Journal of Robotics Research*, **17**, 467–484.

Seraji, H., and Colbaugh, R., 1997, Force tracking in impedance control. *International Journal of Robotics Research*, **16**, 97–117.

Slotine, J.-J. E., and Li, W., 1991, *Applied Nonlinear Control* (Prentice-Hall).

Whitney, D. E., 1977, Force feedback control of manipulator fine motions. *ASME Journal of Dynamic Systems, Measurement and Control*, 91–97.

Whitney, D. E., 1987, Historical perspective and state of the art in robot force control. *International Journal of Robotics Research*, **6**, 3–13.

Whitney, D. E., and Rourke, J. M., 1986, Mechanical behaviour and design equations for elastomer shear pad remote center compliance. *ASME Journal of Dynamic Systems, Measurement and Control*, **108**, 223–232.

Zhang, H., 1989, Kinematic stability of robot manipulators under force control. In *IEEE International Conference on Robotics and Automation*, Scottsdale, AZ, pp. 80–85.